# Coordination-Driven Monolayer-to-Bilayer Transition in 2D Metal-Organic Networks.

*Mina Moradi,[1,2] Nadia L. Lengweiler,[3] Catherine E. Housecroft,[4] Ludovico G. Tulli,[1] Henning Stahlberg,[3] Thomas A. Jung[2*] and Patrick Shahgaldian[1,*]*

[1] Institute of Chemistry and Bioanalytics, School of Life Sciences, University of Applied Sciences and Arts Northwestern Switzerland, Muttenz, Switzerland; Email:

[2] Laboratory for Micro- and Nano-technology, Paul Scherrer Institute, Villigen, Switzerland;

[3] Center for Cellular Imaging and NanoAnalytics (C-CINA), Biozentrum, University of Basel, Basel, Switzerland.

[4] Department of Chemistry, University of Basel, Basel, Switzerland

**Correspondence to:**

**Patrick Shahgaldian –** Email: patrick.shahgaldian@fhnw.ch.

**Thomas A. Jung –** E-mail: thomas.jung@psi.ch

ABSTRACT

We report on monolayer-to-bilayer transitions in 2D metal-organic networks (MONs) from amphiphiles supported at the water air interface. Functionalized calix[4]arenes are assembled through the coordination of selected transition metal ions to yield monomolecular 2D crystalline layers. In the presence of Ni(II) ions, interfacial self-assembly and coordination yields stable monolayers. Cu(II) promotes 2D coordination of a monolayer which is then diffusively re-organizing, nucleates and grows a progressive amount of second layer islands. Atomic force microscopy data of these layers after transfer onto solid substrates reveal crystalline packing geometries with sub-molecular resolution as they are varying in function of the building blocks and the kinetics of the assembly. We assign this monolayer-to-bilayer transition to a diffusive re-organization of the initial monolayers owing to chemical vacancies of the predominant coordination motif formed by $Cu^{2+}$ ions. Our results introduce a new dimension into the controlled monolayer to multilayer architecturing of 2D metal organic networks.

**Keywords:** Monolayer • Bilayer • Calixarene • 2D metal-organic network • Paddle-wheel structure

## Introduction

The controlled construction of well-defined nano-architectures from the bottom up is challenged by the difficulty of restricting self-assembly reactions in a pre-defined dimensionality, *i.e.* as a quantum dot, nanowire or sheet/layer. The challenge is even greater when it comes to the synthesis of bi- or multilayered nanomaterials, for which the self-assembly process must be accurately controlled into the third dimension. Organic and inorganic 2D materials have been widely studied for advanced imaging methods, (opto)electronics, sensing and catalysis.[1] They include graphene,[2] hexagonal boron nitride,[3] transition metal dichalcogenides,[4] metals,[5-6] metal oxides[7] and polymers.[8-9] Design strategies to control single layers have been exploiting supramolecular interactions, transition metal coordination, covalent reactions and combinations thereof.

By exploiting chemical reactions used in polymer chemistry but confined at interfaces, chemists have developed methods to produce covalent organic frameworks (COFs).[10-15] For example, Dichtel *et al*. demonstrated that COF production can be limited to the single layer on single-layer graphene by the reaction of a boronic acid derivative, namely 1,4-phenylene-bis(boronic acid), and hexahydroxy-triphenylene.[12] Schlüter *et al*. demonstrated the possibility of fabricating 2D polymers by reacting, at the air-water interface, a functional amphiphilic monomer composed of three partially fluorinated anthracene units.[14] Recently, Choi *et al*. reported the synthesis of a single layer COF via the photon-assisted imine-condensation of 1,3,5-tris(4-aminophenyl)-benzene and 1,4-benzene-dicarboxaldehyde.[13]

Two-dimensional metal-organic networks (MONs) are typically produced by either top-down (e.g., exfoliation[16]) or bottom-up (e.g., interfacial metal coordination[17-18]) fabrication methods. For example, Nishihara *et al*. reported the formation of π-conjugated nickel bis(dithiolene) complex nanosheets at an organic-inorganic liquid-liquid interface.[18] Feng *et al*. demonstrated the

possibility of producing 2D MONs using a triphenylene-fused nickel bis(dithiolene) complex by means of the Langmuir–Blodgett method.[17] Several self-assembly strategies have enabled the production of single-layer 2D systems without interfacial templating.[11] For example, a complex system combining a water-soluble 2,2'-bipyridine-modified triphenyl-benzene and a cucurbit[8]uril macrocycle was used to produce single-layer 2D supramolecular organic frameworks (SOFs).[19] Stevens *et al*. have demonstrated the fabrication of Janus 2D structures with single-layer thickness by the self-assembly and self-sorting of amphiphilic peptides.[20]

In our efforts to fabricate 2D organic and metal-organic networks, we turned our attention to calix[4]arenes as organic synthons. When designing amphiphilic molecules capable of self-assembly, this class of macrocycles offers key advantages. These include symmetry, moderate conformational rigidity and versatility of chemical modification.[21] We initially focused on calixarenes bearing carboxy groups and long alkyl chains (typically $C_{12}$) attached either at the upper or lower rims of the macrocycle.[22-26] These amphiphilic macrocycles self-assemble at the air-water interface and in water. Their limited propensity to crystallize at interfaces, however, prompted us to turn our attention to calixarene derivatives with shorter alkyl chains ($C_3$).[27-28] Thereby the balance between the van der Waals interactions between the shorter, now less-disordered, alkyl chains and the interactions mediated via the hydrophilic function is significantly reduced and favors interfacial crystallization. On the basis of this building block architecture, we recently fabricated crystalline and freestanding supramolecular organic networks (SONs) of a *p*-methyl-cyano-functionalized calix[4]arene derivative stabilized by weak, yet synergistic, dipole-dipole interactions.[27] Remarkably, those SONs were stable enough to form freestanding, single-layer molecular films. The same macrocycle, bearing carboxylic acid functionalities at the *para*-position, coordinated $Cu^{2+}$ ions at the air-water interface and formed 2D MONs of tunable

crystallinity.[28] To endow the metal-chelating functionalities with more conformational flexibility, we synthesized a calix[4]arene derivative, **1**, bearing *n*-propyl functionalities at the lower rim and methyl-carboxy functionalities at the upper rim (Figure 1A). We herein report our findings on the self-assembly of this amphiphilic derivative as monolayered MONs and their kinetically controlled coordination-driven re-organization to form bilayered architectures.

**Results and discussion**

**Self-assembly at the air-water interface.** 5,11,17,23-Tetramethylcarboxy-25,26,27,28-tetrapropoxy calix[4]arene (**1**) (Figure 1A), locked in the cone conformation by alkylation of the phenol functionalities at low temperature, was synthesized by oxidation of the corresponding tetra-cyano derivative.

The interfacial self-assembly properties of **1** on pure water and aqueous solutions containing 10 $\mu$M $CuCl_2$ or $NiCl_2$ were studied using the Langmuir balance technique and Brewster angle microscopy (BAM). The surface pressure-area compression isotherm shows that **1** does not form a stable monolayer at the air-water interface; the isotherm shows a pseudo-collapse as low as ~3 mN $m^{-1}$ (Figure 1B). However, the limiting area ($A_{lim}$) of 100 $Å^2$ $molecule^{-1}$ determined here is consistent with that measured for other amphiphilic calixarenes.[22-28] This result rules out the partial solubilization of **1** in the water subphase. Thus, the methyl-carboxy rather than the *para*-carboxy derivative hinders intermolecular π-π stacking of neighboring amphiphiles and thereby prevents layer formation. On 10 $\mu$M $NiCl_2$ and $CuCl_2$ solutions in contrast, stable monolayers are evidenced by compression isotherms with collapse pressure ($\pi_c$) values as high as 35 and 42 mN $m^{-1}$, respectively. The stabilization of the layer of **1** in the presence of divalent ions, is reflected by a fairly high $\pi_c$ of 42 mN $m^{-1}$ as compared to 36 mN $m^{-1}$ for the carboxy functionalized analogue on $CuCl_2$. This $\pi_c$ value is remarkably high given the short length of the aliphatic chains and the suspected absence of π-π stacking and can be attributed to the coordination of Cu(II) or Ni(II) ions by the carboxylate moieties. It is worth to note that the value measured on $CuCl_2$ is somewhat low (84 $Å^2$ $molecule^{-1}$) whereas the $A_{lim}$ value measured on $NiCl_2$ of 102 $Å^2$ $molecule^{-1}$ is consistent with a monolayer with the macrocycle $C_4$ pseudo-symmetry axis orthogonal to the surface. This observation prompted us to further study the monolayer behavior of **1**.

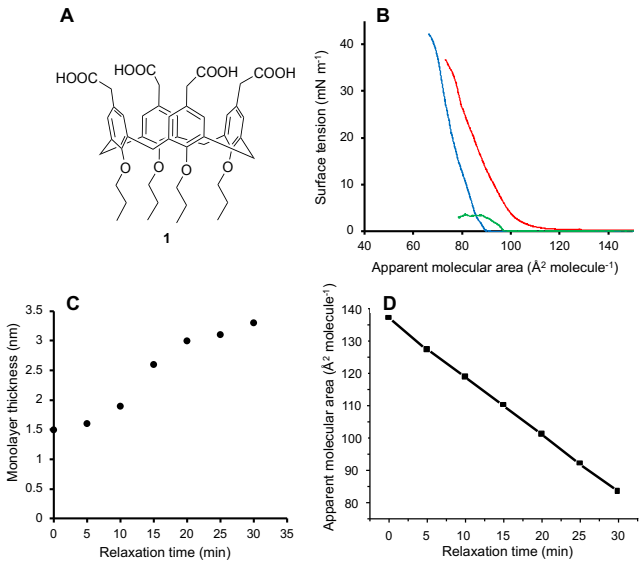


**Figure 1.** Chemical structure and Langmuir monolayer self-assembly. (A) Molecular structure of 5,11,17,23-tetramethylcarboxy-25,26,27,28-tetrapropoxy-calix[4]arene, **1**. (B) Surface pressure-area compression isotherms of **1** on pure water (green) and on aqueous solutions containing 10 $\mu$M aqueous $CuCl_2$ (blue) or 10 $\mu$M $NiCl_2$ (red). (C) Spectroscopic ellipsometry measurement of the average thickness of the compressed monolayer of **1** at $\pi$: 40 mN $m^{-1}$ in the presence of $Cu^{2+}$ ions. The layer was maintained at a surface pressure of 30 mN $m^{-1}$ for 30 min and the layer thickness was measured every 5 min. (D) Stability test of the monolayer of **1** formed at the air-10 $\mu$M $CuCl_2$ solution interface at $\pi$: 40 mN $m^{-1}$.

Brewster Angle Microscopy (BAM) investigations at the air-water interface revealed the typical gas-like and liquid-like phases of the molecular layer before the take-off marked in the surface pressure-area isotherm (Figure S1). Upon further compression, a homogeneous layer is observed. There is no visible structure observed in the BAM images of the self-assembled layer of **1** in presence of either $Cu^{2+}$ or $Ni^{2+}$ (Figure S1). This is contrasting with our recent report on a similar amphiphile but deprived of methylene bridges between the carboxy group and the arene ring, i.e. *p*-carboxy calix[4]arene derivative.[28]

In order to understand the origin of the high $\pi_c$ and low $A_{lim}$ values of the isotherm of **1** in the presence of $Cu^{2+}$ ions, we performed monolayer stability tests and surface ellipsometry measurements. They were carried out by keeping the compressed monolayer at a constant surface

tension of 40 mN $m^{-1}$ on a 10 $\mu$M $CuCl_2$ subphase while recording the loss in molecular area over time (*i.e.*, the response of the layer to the adjusted surface tension over time). Note that this required a continuous adjustment of the position of the Langmuir trough barriers along the course of the experiment. The layer thickness was monitored in real time using spectroscopic ellipsometry (Figure 1). The motion of the barriers over the studied period can, in principle, be attributed to a progressively reduced footprint or 'progressive disappearance' of the molecules on the water subphase. The ellipsometry measurements, however, at the same time show a progressive increase in the monolayer thickness. Indeed, the layer thickness increased from 1.5 nm at the start of the relaxation period to 1.9, 3.0 and 3.3 nm after relaxation durations of 10, 20 and 30 min, respectively. In the case of $NiCl_2$ (instead of $CuCl_2$) in the subphase, the monolayer did not show any comparable behavior and remained stable over the period studied. This set of results suggests that, in the presence of $Cu^{2+}$, the monolayer of **1** undergoes a transition to a bilayer phase.

**Characterization of films transferred on solid substrates.** In order to confirm the bilayer formation hypothesis, we carried out Langmuir–Schaefer (LS) transfers at increasing relaxation durations and analyzed the transferred films by spectroscopic ellipsometry and peak force atomic force microscopy (pfAFM). We used highly oriented pyrolytic graphite (HOPG) as the substrate. In all these experiments, the transfer ratios were measured close to unity, thus confirming successful transfers of the intact layers from the air-water interface onto the HOPG.

pfAFM investigations showed that for samples prepared by transfer without relaxation (*i.e.*, immediately after the surface tension reached the selected value), an LS layer with single-layer thickness fully covered the HOPG surface (Figure 2B).

Our data, in particular for the layer transferred immediately via the LS method, show that several areas of slightly reduced height (~0.5 nm) are visible in addition to the multilayer morphology.

This suggests liquid-expanded phases persisting within a liquid-condensed layer, as previously observed for *p*-acyl-calix[4]arene.[29] Additionally, few brighter islands can be also observed. AFM tip scratching experiments allowed us to measure a layer thickness of $1.3 \pm 0.2$ nm for the LS monolayer and $3.0 \pm 0.5$ nm for the bright islands (Figure S2). The latter value is in good agreement with an LS bilayer of **1**. This finding also adequately explains the ellipsometry results, in which the layer thickness in the Langmuir trough and after LS transfer was measured to be higher than that of a single monolayer. Thus, the layer predominantly comprises a monolayer and a few second-layer islands.

When the transfer onto HOPG is carried out after a longer period of relaxation at the adjusted surface tension value, AFM micrographs revealed an increase in the number and size of the second-layer islands, with bilayer coverage amounting to 10%, 26%, 36%, 63% and 64% of the full layer for relaxation periods of 5, 10, 15, 20 and 25 min, respectively. These results correlate with the optical thickness obtained by ellipsometry at the air-water interface. In combination, AFM and ellipsometry provide convincing evidence that the monolayer-to-bilayer transition occurs under the influence of increased surface tension in the Langmuir trough. This complex equilibration transition progresses continuously over a period in the order of 30 min. It is worth to note that the kinetic evolution is remarkably slow for a process on the level of single molecules occurring at room temperature. The equilibration level is reached at different morphology endpoints and second-layer island densities depending on the chosen surface tension. Interestingly, this transition occurs only at the air-water interface and is discontinued after LS transfer of the film onto the solid substrate. In comparison to earlier reports[30, 31] on the morphology of Langmuir monolayer collapse, it is remarkable that for the present system, there are no indications of collapse at the surface pressure increase used in these experiments. Also in contrast we observe a kinetically controlled

evolution of the layer morphology which resembles nucleation and growth kinetics[32] during thin film deposition (Figure 2 ).

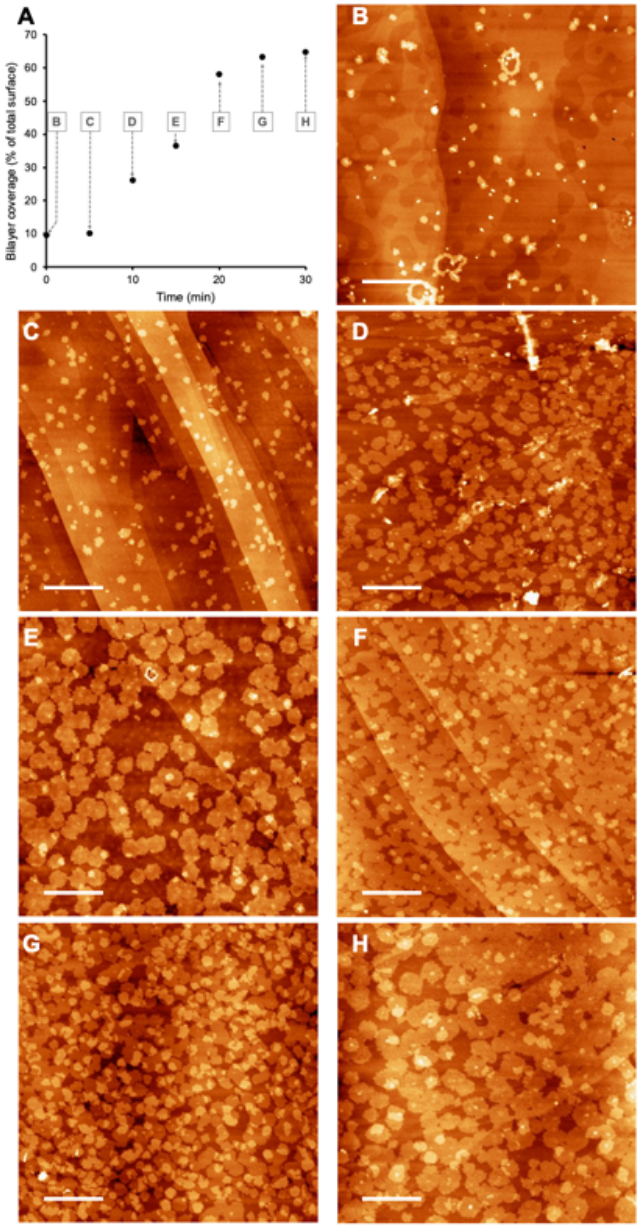


**Figure 2.** Peak-force atomic force microscopy (pfAFM) study of the temporal evolution of the LS layer and island morphology after increasing the surface tension set point. Langmuir monolayers of **1** have been transferred at different time points at a surface tension of 40 mN $m^{-1}$. Layers were transferred via the LS method from the interface of a 10 $\mu$M $CuCl_2$ solution onto freshly cleaved HOPG substrates. The fraction of bi/multilayer islands depicted by pfAFM (A) increases with increasing time to transfer: (B) 0 min, (C) 5 min (D) 10 min, (E) 15 min, (F) 20 min, (G) 25 min and (H) 30 min.

We also carried out additional high-resolution AFM investigations of the films transferred from the $CuCl_2$ and $NiCl_2$ solutions described above; representative micrographs are presented in Figure 3.

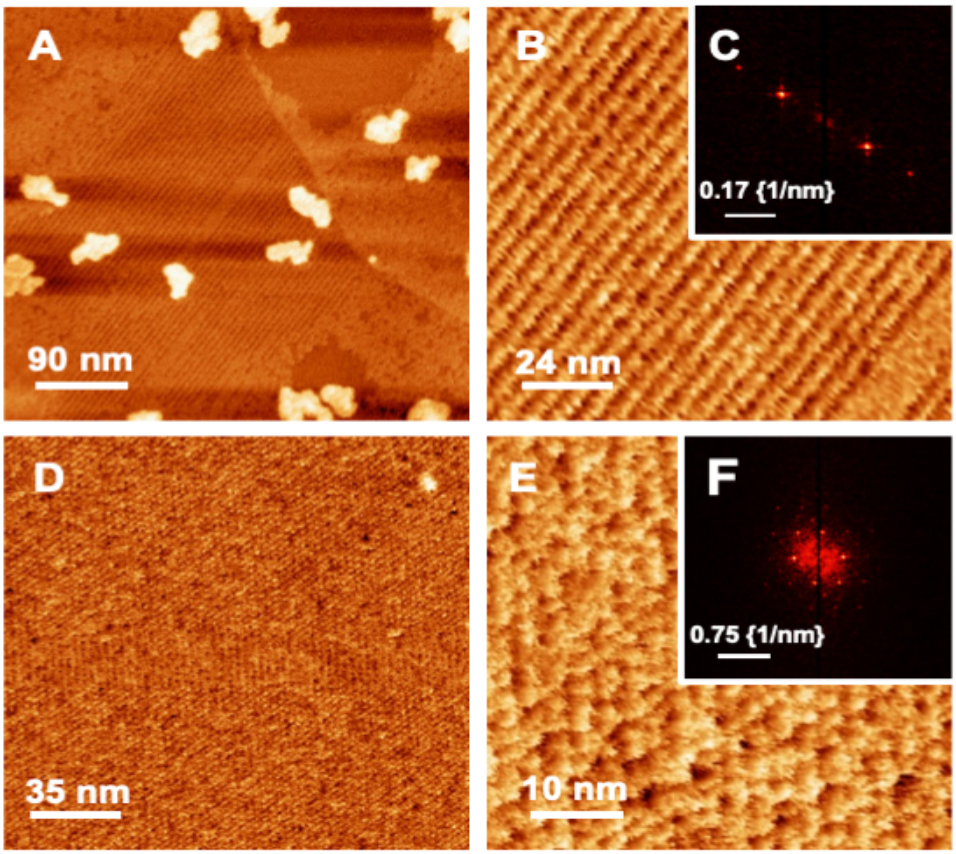


**Figure 3.** Molecular-resolution atomic force microscopy (AFM) micrographs of the transferred layers showing different crystalline patterns and second-layer islands: AFM data taken after transfer of **1** via the LS method from the interface of 10 $\mu$M $CuCl_2$ (A & B) and $NiCl_2$ (D & E) solutions. The fast Fourier transform analysis of the AFM micrographs of the crystalline layers is shown in C & F.

These BAM and AFM data consistently reveal that the monolayer assembled on the $CuCl_2$ subphase exhibits crystalline (appearing as stripes) and amorphous domains (Figure 3A &B). 2D fast Fourier transformations (FFT) performed on the AFM micrographs of the crystalline stripe patterns identify a periodicity of ~5 nm (Figure 3C). The crystalline domains of the layer of **1** upon interaction with $Cu^{2+}$ ions have the same width and morphology as those reported for the MON of

the *para*-carboxylate derivative.[28] In contrast, AFM analysis of samples transferred after assembly on $NiCl_2$ solutions shows a completely different morphology: domains of the highly crystalline monolayer of **1** are found across large areas (up to 4×4 $\mu$m). Even after repeated sample preparation and by screening large sample areas, no bilayer islands were found in this case (Figure 3D & 3E). 2D FFT analysis of the molecular-resolution AFM image revealed a rhombohedral unit cell size of ~2 nm for the network of **1** and $Ni^{2+}$ (Figure 3F), which is consistent with the expected size of the macrocycle of **1** in a pinched cone conformation.

We performed cryo-transmission electron microscopy (TEM) investigations for the MON of **1** transferred onto lacey carbon copper TEM grids (Figure 4). Our results confirm that the MON of **1** is homogeneous, freestanding and sufficiently mechanically stable to span holes as large as $4 \times 4\ \mu$m. TEM analysis of the transferred MON of **1** from a $CuCl_2$ solution provides clear evidence for the bilayer structure. Transferring MON of **1** after 30 min relaxation time reveals a higher surface coverage with bilayer islands. Our TEM analysis thus provides further evidence of kinetic control of the multilayer architecture as a function of the time between preparation and transfer of the LS layer.

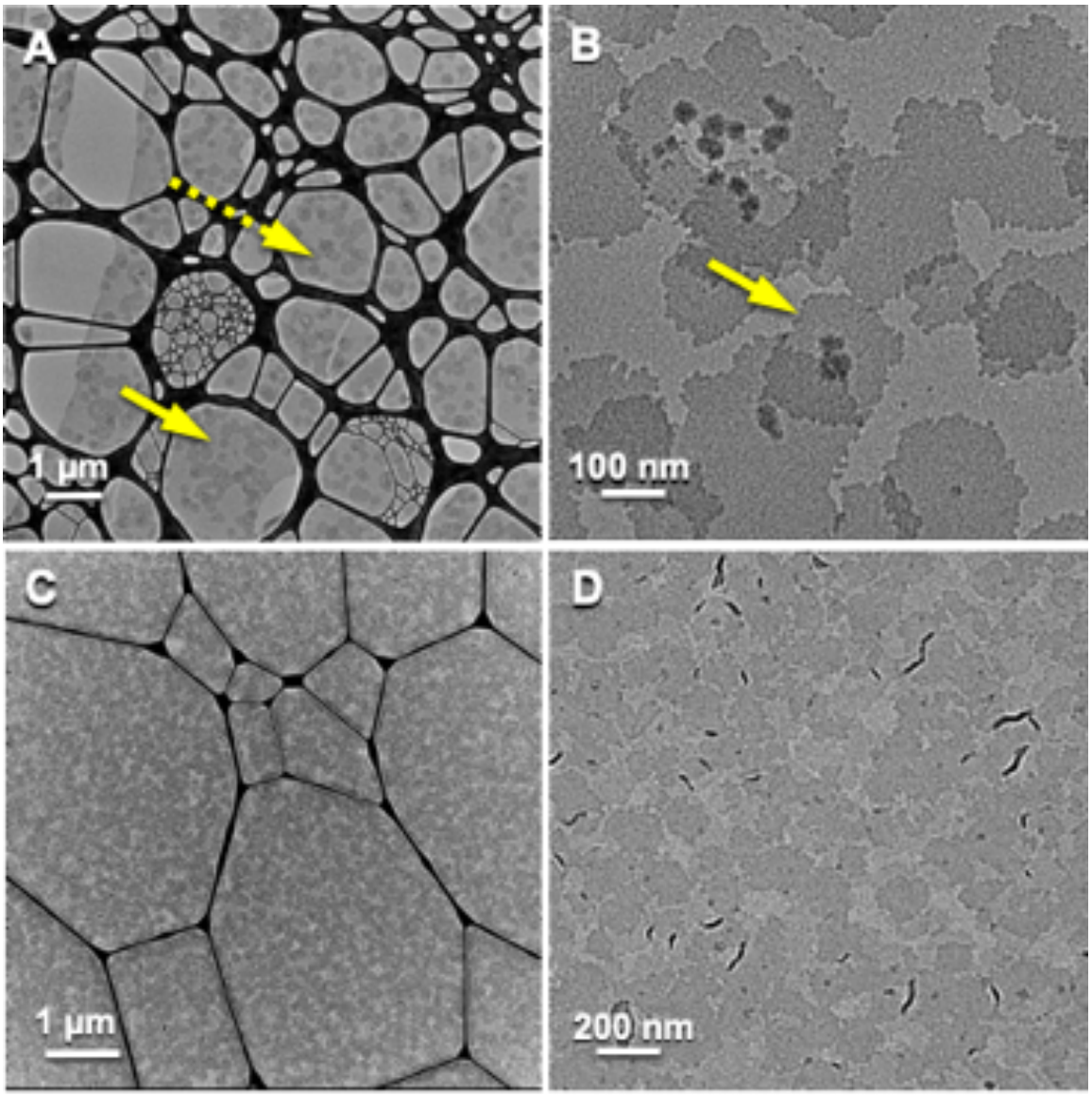


**Figure 4.** Cryo-EM imaging of the transferred 2D MON of 1 via the LS method to the lacey carbon grid from a 10 $\mu$M of CuCl2, yellow arrows indicate: (- -) bilayer and (-) monolayer (A) as well as boundary between the monolayer and bilayer (B). The layer is free-standing over as large area as 4 $\mu$m × 4 $\mu$m (C). TEM analysis reveals that degree of bilayer formation improved drastically after 30 min relaxation time (C&D).

The produced and transferred layers were further characterized by *X*-ray photoelectron spectroscopy (XPS) in order to assess the chemical bonds formed between the carboxyl groups and transition metal ions and their stoichiometry (Figure 5). Coordination bonds between the

carboxyl groups of **1** and the ions were identified by analyzing the C1s, Cu2p, Ni2p and Cl2p spectra presented in Table S1 and Figure S3 & S4, consistent with our earlier report.[28] Further evidence of the different bonding in the copper and nickel coordination nodes of the organic network of **1** lies in the position of the carboxylic peak, which is shifted by 0.5 eV between nickel and copper coordination (Figure 5B). These values are in agreement with a paddle-wheel coordination geometry for carboxy-copper systems[33] and with an octahedral geometry for carboxy-nickel systems.[34]

In the MON containing **1**, the average ratio between the carboxyl groups and the copper and nickel nodes was ~1:1 and 4:1, respectively. The ~1:1 ratio of carboxy functional groups to copper nodes is consistent with the bilayer formation of **1** via a paddle-wheel carboxy-copper geometry. This motif, $\{Cu_2(RCO_2)_4\}$, is very common for copper(II) carboxylato coordination compounds in both discrete and extended systems. This is confirmed by a search of the Cambridge Structural Database (CSD[35] v. 5.41, searched using Conquest v. 2020.1[36]), which produced almost 1600 hits for a $\{Cu_2(RCO_2)_4\}$ unit. In contrast, only 45 analogous $Ni^{2+}$-containing paddle-wheel units have been structurally characterized. Instead, octahedral $\{NiO_6\}$ are typical with monodentate O- or bidentate O,O'-ligands or in multinuclear assemblies. Consistent with this finding, the 4:1 ratio between the carboxy and the nickel groups observed for the MON of **1** coordinated with $Ni^{2+}$ ions suggests an octahedral coordination geometry of nickel and carboxy linkers of neighboring amphiphiles.

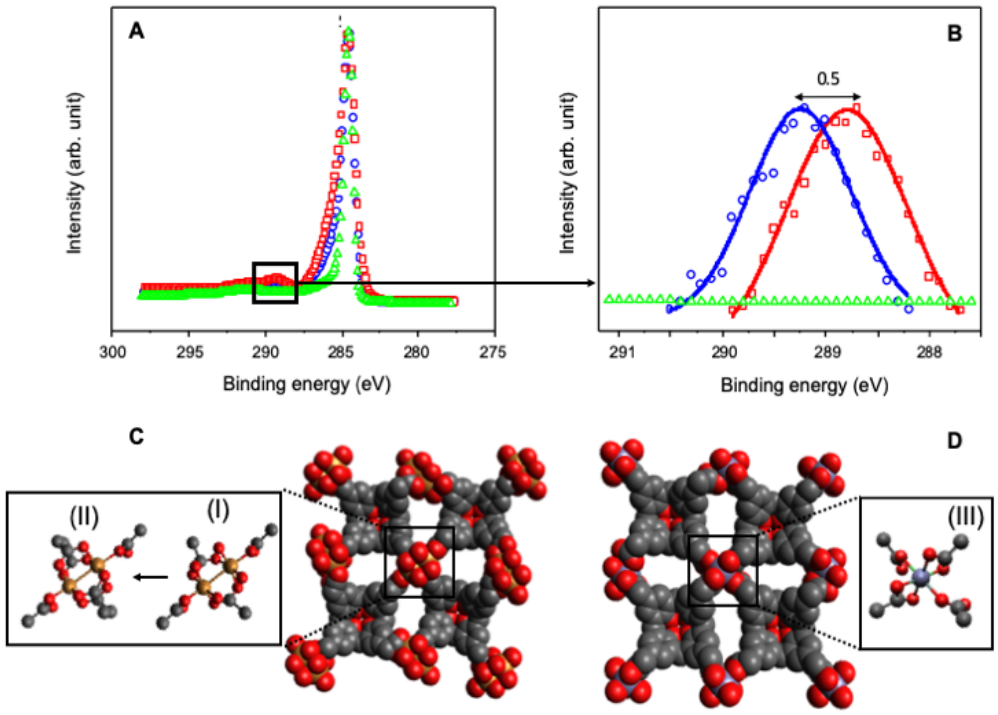


**Figure 5.** Surface analysis to identify the coordination stoichiometry between the calixarene COOH and the coordination metal. XPS spectra of the C1s peak of the MON of **1** after the LS transfer onto HOPG. Data are shown for layers transferred from 10 μM aqueous solutions of $CuCl_2$ (red) and $NiCl_2$ (blue). Clean HOPG (green) is shown as reference (A). Normalized C1s spectra in the carboxylic region after background subtraction. The carboxy carbon C1s peak positions in the MON of **1** were 288.8 and 289.2 eV for copper and nickel coordination, respectively (B). (C) and (D). Proposed molecular models of the network of **1** coordinated with copper and nickel, respectively, hydrogen atoms are omitted for clarity. I, II show a detailed view of the paddle-wheel Cu(II) coordination geometry and III and the octahedral coordination of Ni(II).

Based on the results of interfacial studies, AFM, TEM and XPS, we propose packing models for the MON of **1** coordinated with $Cu^{2+}$ and $Ni^{2+}$ ions (Figure 5C & 5D). The proposed molecular models of the network of **1** coordinated with copper comprises a coordination node in the paddle-wheel arrangement (I). Note that the axis of the paddle-wheel in (I) is oriented parallel with regard to the calixarene layer and only two paddle-wheels are coordinated to the copper dimer, with water taking the role of the other two paddle-wheels. This also explains the stronger anisotropy of the

Cu coordinated layer in comparison to the Ni coordinated layer in our high resolution AFM data (Fig. 3b, 3). Bilayer formation occurs upon coordination of the flipped amphiphiles of **1** into the subphase, replacing water molecules in the coordination sphere and thereby forming the fully coordinated motif (II) as it has also been found in 3D space filling metal organic frameworks.[37] Thereby, a third and fourth paddle-wheel are coordinated, possibly in conjunction with the formation of supramolecular capsules. The octahedral coordination arrangement of **1** with nickel comprises two bidentate (from the open rings of the pinched cone conformation of 1) and two monodentate carboxy ligands (from the close-to-parallel rings) (III), consistent with the observation of the MON of 1 only in the monolayer form. Importantly, the nickel coordination sphere does not offer vacancies in the form of replaceable water molecules for the coordination of **1** in a 3D motif. Thereby, the comparably slow kinetic relaxation of the layers after adjusting higher surface pressures appears to be a combined effect of the reduced dimensionality (compared to diffusive processes at liquid-layer interfaces) and the probably high complexity of the configurational / conformational trajectory for a single molecule to reach a second layer position by diffusion. Such processes, even for rather simple molecules held in 2D confinements are typically co-determined by complex enthalpy-entropy balancing[38,39] and can be very slow, as reported earlier.[40]

**Conclusion**

We have demonstrated the formation of crystalline, metal-organic coordination networks using a calixarene building block bearing conformationally flexible carboxylate moieties and copper (II) or nickel (II) coordination metal ions. The rational choice of the organic building block and the metal ion node allows producing a bilayered metal organic network in surface/interface supported and free-standing form. The specific paddle-wheel coordination motif forming the copper-

coordinated network layer offers degrees of freedom that facilitate a kinetically controlled monolayer-to-bilayer transition at increased surface pressure.

Thorough investigation of the bilayer formation process has been carried out by means of Langmuir compression experiments, surface ellipsometry, XPS, cryo-TEM and high-resolution AFM. Our results unambiguously show a diffusive re-organization of the initial monolayer constituents through a coordination-driven and kinetically controlled process yielding bilayered materials. Additional cryo-TEM experiments also bring evidence that the bilayer networks are of sufficient stability to be transferred as freestanding films spanning areas as large as 4 x 4 μm. Our here presented, first report of this phenomenon suggests further investigations on related molecules and the detailed assessment of thermodynamic and kinetic factors, This approach is versatile in that it can be applied to a variety of amphiphiles thereby allowing the systematic design of functional bilayered metal-organic networks and thereby significantly extends the library of physicochemical methods to fabricate functional layers for catalysis, electrochemistry and sensing among other applications

**Experimental section**

Solvents and chemicals were purchased from Merck (Switzerland) and used without further purification. 5,11,17,23-Tetra-methyl-carboxy-25,26,27,28-tetra-propoxy calix[4]arene (**1**) was synthetized following the literature procedure.[41] Nanopure water was produced using a Millipore ®Synergy purification system with a resistivity of 18 MΩ cm.

A Nima (Coventry, UK) 112D Langmuir trough was used to perform surface pressure-area compression isotherms. For all experiments, the trough and barriers were cleaned with analytical

grade chloroform and nanopure water. Aqueous solutions of 10 $\mu$M $CuCl_2$ and 10 $\mu$M $NiCl_2$ were used as subphases. A solution of **1** (13 μL, 0.5 mg $mL^{-1}$ in chloroform) was spread at the air-liquid interface using a gastight microsyringe. After 15 min solvent evaporation and equilibration of amphiphiles at the interface, barriers were symmetrically closed at a speed rate of 5 $cm^2$ $min^{-1}$. Experiments were carried out in triplicates, measurement accuracy was at least ± 0.1 mN $m^{-1}$ and ±1 $Å^2$ $molecule^{-1}$, for surface tension and apparent molecular area values, respectively.

Highly oriented pyrolytic graphite (HOPG) and hydrophobic silicon wafers (coated with octadecyltrichlorosilane, OTS)[23] were used as solid substrates for the Langmuir-Schaefer (LS) transfers, using a Nima deposition system. The speed of substrates approaching the interface was 1 mm $min^{-1}$. LS transfer of layers of **1**, prepared on 10 $\mu$M $CuCl_2$ and a 10 $\mu$M $NiCl_2$ solutions, were transferred onto the solid substrates at 40 and 30 mN $m^{-1}$, respectively. The substrates were slowly removed from the aqueous solution, after 15 min, at a constant speed of 1 mm $min^{-1}$.

Nanofilm_ep3 system Accurion (Germany) equipped with an internal solid-state laser at a wavelength of 658 nm was used to perform Brewster angle microscopy and ellipsometry. The images were acquired using a CCD camera (768 × 562 pixels) and a 10× magnification objective, equipped with an automatic focus scanner yielding 1 μm lateral resolution. Ellipsometry analyses were carried out in a nulling polarizer-compensator-sample-analyzer set-up. In the ellipsometry measurements the refractive index of **1** was considered 1.5.[42] OTS-coated silicon wafers were used as solid substrates for the LS transfer in the ellipsometry experiments.

Monochromatic Al $K_\alpha$ ($h\nu$=1486.7 eV) excitation source (Specs FOCUS 500) in normal emission using a Specs PHOIBOS 150 electron analyzer was used to perform *X*-ray photoelectron spectroscopy (XPS). The C1s core level of HOPG, 284.5 eV, was used as reference for the binding

energies. The measurements were carried out in a ultra-high vacuum system with base pressure of $10^{-11}$ mbar.

Atomic force microscopy in the PeakForce® mode using a Multimode 8 instrument (Bruker) equipped with a Nanoscope V controller was used for imaging and height analysis of the transferred 2D-MON of **1** from the interface onto a HOPG. Scanasyst-air-HR silicon tips on silicon nitride lever were used for high-resolution AFM imaging.

LS layers of **1** were transferred from the air-solution interface onto a lacey-carbon-covered copper electron microscopy grids (Ted Pella, USA) via the Langmuir-Schaefer transfer procedure as developed and described before.[27] Transmission electron microscopy (TEM) imaging was performed in the low dose mode, under cryo-conditions (the EM grid has been placed onto the cryoholder at room temperature, inserted to the microscope and cooled down with liquid nitrogen before exposure to the electrons) to provide better stability to the electron beam. Images were recorded with a Talos-200C (FEI) transmission electron microscope, operated at an accelerating voltage of 200 keV. The highly defocused images were collected using a FEI Ceta 16 MPixel CMOS camera.

ASSOCIATED CONTENT

**Supporting Information**.

The Supporting Information is available free of charge at:

Brewster angle micrographs, further AFM characterization and X-ray photoelectron spectroscopy.

AUTHOR INFORMATION

**Corresponding Authors**

**Patrick Shahgaldian –** University of Applied Sciences and Arts Northwestern Switzerland, School of Life Sciences, Institute of Chemistry and Bioanalytics, Muttenz, Switzerland; Email: patrick.shahgaldian@fhnw.ch.

**Thomas A. Jung –** Paul Scherrer Institute, Laboratory for Micro- and Nano-technology, Villigen, Switzerland; Email: thomas.jung@psi.ch

**Other Authors**

**Mina Moradi, Ludovico G. Tulli –** University of Applied Sciences and Arts Northwestern Switzerland, School of Life Sciences, Institute of Chemistry and Bioanalytics, Muttenz, Switzerland.

**Nadia L. Lengweiler, Henning Stahlberg –** Center for Cellular Imaging and NanoAnalytics (C-CINA), Biozentrum, University of Basel, Basel, Switzerland.

**Catherine E. Housecroft –** Department of Chemistry, University of Basel, Basel, Switzerland

## Author Contributions

MM, TAJ and PS conceived and designed the experiments. MM, NLL and LGT carried out the experimental work. NLL and HS analyzed the cryo-EM results. MM, TAJ, PS and CEH designed the molecular two-dimensional packing model. The manuscript was written through contributions of all authors. All authors have given approval to the final version of the manuscript.


## Acknowledgements

The authors would like to thank Dr. Milos Baljozovic for interesting and helpful discussions on the XPS data and analysis.

## Funding Sources

The financial support of the Swiss Nanoscience Institute (grant P1305 and P1308) is gratefully acknowledged. T.A.J. acknowledges the Swiss National Science Foundation (grant nos. 200020-153549, 200020-175800, 206021_144991 and 206021-113149). The authors are also grateful to the Paul Scherrer Institute, the Physics Department of the University of Base,l the Swiss Commission for Technology and Innovation (CTI, 16465.1 PFNM-NM) and the Swiss Government Excellence Scholarship Program for Foreign Scholars. AFM and XPS measurements were performed at the Laboratory for Micro- and Nanotechnology at the Paul Scherrer Institute (PSI).

REFERENCES


1. Dong, R.; Zhang, T.; Feng, X., Interface-assisted synthesis of 2D materials: trend and challenges. *Chem. Rev.* **2018,** *118*, 6189-6235.
2. Geim, A. K.; Novoselov, K. S., The rise of graphene. *Nat. Materials* **2007,** *6*, 183-91.
3. Weng, Q.; Wang, X.; Wang, X.; Bando, Y.; Golberg, D., Functionalized hexagonal boron nitride nanomaterials: emerging properties and applications. *Chem. Soc. Rev.* **2016,** *45*, 3989-4012.
4. Li, H.; Li, Y.; Aljarb, A.; Shi, Y.; Li, L. J., Epitaxial growth of two-dimensional layered transition-metal dichalcogenides: growth mechanism, controllability, and scalability. *Chem. Rev.* **2018,** *118*, 6134-6150.
5. Duan, H.; Yan, N.; Yu, R.; Chang, C. R.; Zhou, G.; Hu, H. S.; Rong, H.; Niu, Z.; Mao, J.; Asakura, H.; et. al., Ultrathin rhodium nanosheets. *Nat. Commun.* **2014,** *5*, 3093.
6. Huang, X.; Li, S.; Huang, Y.; Wu, S.; Zhou, X.; Li, S.; Gan, C. L.; Boey, F.; Mirkin, C. A.; Zhang, H., Synthesis of hexagonal close-packed gold nanostructures. *Nat. Commun.* **2011,** *2*, 292.
7. Xiao, X.; Song, H.; Lin, S.; Zhou, Y.; Zhan, X.; Hu, Z.; Zhang, Q.; Sun, J.; Yang, B.; Li, T.; et al., Scalable salt-templated synthesis of two-dimensional transition metal oxides. *Nat. Commun.* **2016,** *7*, 11296.
8. Champness, N. R., Surface chemistry: Making the right connections. *Nat. Chem.* **2012,** *4*, 149-50.
9. Kissel, P.; Erni, R.; Schweizer, W. B.; Rossell, M. D.; King, B. T.; Bauer, T.; Gotzinger, S.; Schluter, A. D.; Sakamoto, J., A two-dimensional polymer prepared by organic synthesis. *Nat. Chem.* **2012,** *4*, 287-91.
10. Bilbao, N.; Martin, C.; Zhan, G.; Martinez-Abadia, M.; Sanz-Matias, A.; Mateo-Alonso, A.; Harvey, J. N.; Van der Auweraer, M.; Mali, K. S.; De Feyter, S., Anatomy of on-surface synthesized boroxine two-dimensional polymers. *ACS Nano* **2020,** *14*, 2354-2365.
11. Colson, J. W.; Dichtel, W. R., Rationally synthesized two-dimensional polymers. *Nat. Chem.* **2013,** *5*, 453-65.
12. Colson, J. W.; Woll, A. R.; Mukherjee, A.; Levendorf, M. P.; Spitler, E. L.; Shields, V. B.; Spencer, M. G.; Park, J.; Dichtel, W. R., Oriented 2D covalent organic framework thin films on single-layer graphene. *Science* **2011,** *332*, 228-31.
13. Kim, S.; Lim, H.; Lee, J.; Choi, H. C., Synthesis of a scalable two-dimensional covalent organic framework by the photon-assisted imine condensation reaction on the water surface. *Langmuir* **2018,** *34*, 8731-8738.
14. Muller, V.; Hinaut, A.; Moradi, M.; Baljozovic, M.; Jung, T. A.; Shahgaldian, P.; Mohwald, H.; Hofer, G.; Kroger, M.; King, B. T.; et al., A two-dimensional polymer synthesized at the air/water interface. *Angew. Chem. Int. Ed.* **2018,** *57*, 10584-10588.

15. Payamyar, P.; King, B. T.; Ottinger, H. C.; Schluter, A. D., Two-dimensional polymers: concepts and perspectives. *Chem. Commun.* **2016,** *52*, 18-34.

16. Zhao, M.; Huang, Y.; Peng, Y.; Huang, Z.; Ma, Q.; Zhang, H., Two-dimensional metal-organic framework nanosheets: synthesis and applications. *Chem. Soc. Rev.* **2018,** *47*, 6267-6295.

17. Dong, R.; Pfeffermann, M.; Liang, H.; Zheng, Z.; Zhu, X.; Zhang, J.; Feng, X., Large-area, free-standing, two-dimensional supramolecular polymer single-layer sheets for highly efficient electrocatalytic hydrogen evolution. *Angew. Chem. Int. Ed.* **2015,** *54*, 12058-63.

18. Kambe, T.; Sakamoto, R.; Hoshiko, K.; Takada, K.; Miyachi, M.; Ryu, J. H.; Sasaki, S.; Kim, J.; Nakazato, K.; Takata, M.; et al., pi-Conjugated nickel bis(dithiolene) complex nanosheet. *J. Am. Chem. Soc.* **2013,** *135*, 2462-5.

19. Zhang, K. D.; Tian, J.; Hanifi, D.; Zhang, Y.; Sue, A. C.; Zhou, T. Y.; Zhang, L.; Zhao, X.; Liu, Y.; Li, Z. T., Toward a single-layer two-dimensional honeycomb supramolecular organic framework in water. *J. Am. Chem. Soc.* **2013,** *135*, 17913-8.

20. Lin, Y.; Thomas, M. R.; Gelmi, A.; Leonardo, V.; Pashuck, E. T.; Maynard, S. A.; Wang, Y.; Stevens, M. M., Self-sssembled 2D free-standing Janus nanosheets with single-layer thickness. *J. Am. Chem. Soc.* **2017,** *139*, 13592-13595.

21. Tulli, L. G.; Shahgaldian, P., Calixarenes and Resorcinarenes at Interfaces. In *Calixarenes and Beyond*, Neri, P.; Sessler, J. L.; Wang, M.-X., Eds. Springer: Cham, 2016; pp 987-1010.

22. Moridi, N.; Elend, D.; Danylyuk, O.; Suwinska, K.; Shahgaldian, P., Amidophenol-Modified Amphiphilic Calixarenes: Synthesis, Interfacial Self-Assembly, and Acetaminophen Crystal Nucleation Properties. *Langmuir* **2011,** *27*, 9116-9121.

23. Moridi, N.; Wackerlin, C.; Rullaud, V.; Schelldorfer, R.; Jung, T. A.; Shahgaldian, P., Langmuir-Blodgett monolayer stabilization using supramolecular clips. *Chem. Commun.* **2013,** *49*, 367-9.

24. Rullaud, V.; Moridi, N.; Shahgaldian, P., Sequence-Specific DNA Interactions with Calixarene-Based Langmuir Monolayers. *Langmuir* **2014,** *30*, 8675-8679.

25. Tulli, L. G.; Moridi, N.; Wang, W.; Helttunen, K.; Neuburger, M.; Vaknin, D.; Meier, W.; Shahgaldian, P., Polymorphism control of an active pharmaceutical ingredient beneath calixarene-based Langmuir monolayers. *Chem. Commun.* **2014,** *50*, 3938-40.

26. Tulli, L. G.; Wang, W.; Lindemann, W. R.; Kuzmenko, I.; Meier, W.; Vaknin, D.; Shahgaldian, P., Interfacial binding of divalent cations to calixarene-based Langmuir monolayers. *Langmuir* **2015,** *31*, 2351-9.

27. Moradi, M.; Opara, N. L.; Tulli, L. G.; Wackerlin, C.; Dalgarno, S. J.; Teat, S. J.; Baljozovic, M.; Popova, O.; van Genderen, E.; Kleibert, A.; et al., Supramolecular architectures of molecularly thin yet robust free-standing layers. *Sci. Adv.* **2019,** *5*, eaav4489.

28. Moradi, M.; Tulli, L. G.; Nowakowski, J.; Baljozovic, M.; Jung, T. A.; Shahgaldian, P., Two-dimensional calix[4]arene-based metal-organic coordination networks of tunable crystallinity. *Angew. Chem. Int. Ed.* **2017,** *56*, 14395-14399.

29. Shahgaldian, P.; Cesario, M.; Goreloff, P.; Coleman, A. W., Para-acyl calix[4]arenes: amphiphilic self-assembly from the molecular to the mesoscopic level. *Chem. Commun.* **2002**, 326-7.

30. Ries, H. E., Stable ridges in a collapsing monolayer. *Nature* **1979,** *27*, 287-289

31. Lee, K.Y.C., Collapse mechanisms of Langmuir monolayers. *Annu. Rev. Phys. Chem.* **2008,** *59*, 771-791.

32. Oura, K.; Lifshits, V. G.; Saranin, A.; Zotov, A. V.; Katayama, M. *Surface Science - An Introduction*, Springer, 2003.

33. Wang, Y.; Zhang, C.; Li, H.; Zhu, G.; Bao, S. S.; Wei, S.; Zheng, L. M.; Ren, M.; Xu, Z., Synthesis, characterization and in vitro anticancer activity of the biomolecule-based coordination complex nanotubes. *J. Mater. Chem. B* **2015,** *3*, 296-305.

34. Kishi, K.; Ehara, Y., Interaction of acetic acid with ethylenediamine on a Ni(111) surface studied by XPS. *Surf. Sci.* **1986,** *176*, 567-577.

35. Groom, C. R.; Bruno, I. J., Lightfoot, M. P.; Ward, S. C., The Cambridge Structural Database. *Acta Crystallogr. B* **2016,** *72*, 171-9.

36. Bruno, I. J.; Cole, J. C.; Edgington, P. R.; Kessler, M.; Macrae, C. F.; McCabe, P.; Pearson, J.; Taylor, R., New software for searching the Cambridge Structural Database and visualizing crystal structures. *Acta Crystallogr. B* **2002,** *58*, 389-97.

37. Koeberl, M.; Cokoja, M.; Herrmann, W. A.; Kuehn, F. E., From molecules to materials: molecular paddle-wheel synthons of macromolecules, cage compounds and metal–organic frameworks. *Dalton Trans.* **2011**, *40*, 6834-6859.

38. Wintjes, N.; Lobo-Checa, J.; Hornung, J.; Samuely, T.; Diederich, F.; Jung, T. A., Two-dimensional phase behavior of a bimolecular porphyrin system at the solid–vacuum interface. *J. Am. Chem. Soc.* **2010,** *132*, 7306-7311.

39. Wintjes, N.; Hornung, J.; Lobo-Checa, J.; Voigt, T.; Samuely, T.; Thilgen, C.; Stöhr, M.; Diederich, F.; Jung, T. A., Supramolecular synthons on surfaces: controlling dimensionality and periodicity of tetraarylporphyrin assemblies by the interplay of cyano and alkoxy substituents. *Chem. Eur. J.* **2008,** *14*, 5794 - 5802.

40. Samuely, T.; Liu, S.-X.; Wintjes, N.; Haas, M.; Decurtins, S.; Jung, T. A.; Stöhr, M., Two-Dimensional multiphase behavior induced by sterically hindered conformational optimization of phenoxy-substituted phthalocyanines. *J. Phys. Chem. C* **2008**, *112*, 6139-6144.

41. Sharma, S. K.; Kanamathareddy, S.; Gutsche, C. D., Upper rim substitution of calixarenes: carboxylic acids. *Synthesis* **1997,** *11*, 1268-1272.

42. Shirshov, Y. M.; Zynio, S. A.; Matsas, E. P.; Beketov, G. V.; Prokhorovich, A. V.; Venger, E. F.; Markovskiy, L. N.; Kalchenko, V. I.; Soloviov, A. V.; Merker, R., Optical parameters of thin calixarene films and their response to benzene, toluene and chloroform adsorption. *Supramol. Sci.* **1997,** *4*, 491-494.

TOC GRAPHIC